Approaches to gel electrolytes in dye-sensitized solar cells using pyridinium molten salts

Cheng-Hsien Yang,*[a] Wen-Yueh Ho,[b] Hao-Hsun Yang[a] and Mao-Lin Hsueh[a]

Received 23rd February 2010, Accepted 29th April 2010
DOI: 10.1039/c0jm00485e

Imidazolium iodide ionic liquids have a relatively high viscosity, and, as consequence, mass-transport limitation problems restrict their use as solvents for electrolytes. In this study, a series of 1-alkyl-3-carboxypyridinium iodide molten salts, [ACP][I], was used as a gel electrolyte for dye-sensitized solar cells (DSSCs). Without addition of any nano-particles, small molecules, oligomers or polymer plasticizers, these [ACP][I] salts acted as a stiffener, plasticizing the liquid phase electrolyte. An investigation was carried out into the electrochemical properties of these [ACP][I]-based gel electrolytes, and they were found to have an impressively high diffusion constant ($D_{I_3^-}$) of ~28.5 × 10^{-6} cm^2 s^{-1} and conductivity (σ) of ~4.30 mS cm^{-1}. The photovoltaic performance of this new redox couple was evaluated by employing nanocrystalline TiO_2 films with different thicknesses. An energy conversion efficiency of 3.7% was achieved using an 8 μm TiO_2 electrode, under simulated solar illumination (AM 1.5, 100 mW cm^{-2}). This efficiency is comparable with the cells fabricated with the liquid electrolyte-Solaronix AN-50 (η 4.0%, reported in the literature).

Introduction

Dye-sensitized solar cells have attracted considerable academic and industrial research interest since O'Regan and Gratzel's report in 1991.[1] Usually these cells consist of a working electrode which is coated with a dye-sensitized mesoporous film of nano-crystalline particles of TiO_2, a Pt-coated counter electrode and an electrolyte containing a suitable redox couple. The functioning of such devices is based on the electron injection from the photo-excited state of the dye molecule into the conduction band of the TiO_2, followed by regeneration of the dye by an iodide/triiodide (I^-/I_3^-) redox couple. Typically, high power conversion efficiencies (η) of more than 11% have been achieved by using volatile solvent-based electrolytes.[2] However, there are some problems associated with the presence of these electrolytes, including electrolyte encapsulation, electrolyte leakage and cell deterioration,[3–5] and these severely restrict practical industrial applications.

There are two potential materials for the electrolyte system. Polymer electrolytes are solid conductors prepared by the dissolution of salts in suitable polymer substrates, and play a crucial role in improving the ionic conductivity and mechanical stability of DSSCs.[6] Although the solid-state nature of polymer electrolytes is an advantage for fabricating DSSCs, their ionic conductivity is too low for applications in photoelectrochemical cells. Potential alternatives to volatile solvents are non-volatile, room-temperature ionic liquids (ILs).[7] ILs-based electrolytes are attractive because of their almost zero vapor pressure, wide electrochemical window, non-flammability and high stability to chemicals and light. However, the high viscosity of ionic liquids appears to restrict their use because of transport limitations.[8,9] In order to compensate for their slow diffusion, a higher I_3^- concentration is needed.[10] However, the diffusion coefficients of I_3^- in ionic liquid electrolytes are still about 1–2 orders of magnitude lower than those in volatile solvents.

In this study, we explored the possibility of using a series of molten salts – 1-alkyl-3-carboxypyridinium iodides, [ACP][I] – to take the place of room-temperature ionic liquids, polymers and stiffeners to plasticize the liquid-phase electrolyte. To the best of our knowledge, this kind of gel electrolyte has not yet been applied to DSSCs. Electrochemical impedance spectroscopy (EIS) and cyclic voltammetry (CV) were used to evaluate the role of the [ACP][I] salts in gel electrolytes and DSSCs. These gel electrolytes have an unprecedented diffusion constant ($D_{I_3^-}$) of 28.5 × 10^{-6} cm^2 s^{-1}, and a power conversion efficiency of 5.3% under full air-mass (AM 1.5) sunlight.

Results and discussion

Synthesis and gelation properties of electrolytes

One of the most outstanding characteristics of small-molecule organic materials is their adjustable molecular structure, which can be used to alter the physical and chemical properties of the compound. Considering that the imidazolium-based and pyridinium-based ionic liquids are high-performance electrolytes in DSSCs, a carboxyl group was introduced into the pyridinium-type ionic conductor to form the [ACP][I] salts in this work. These [ACP][I] salts were synthesized by quaternization reactions of pyridine-3-carboxylic acid with two equivalents of the alkyl iodide, as shown in Scheme 1.[11] The carboxyl group of molecules produced strong intermolecular hydrogen bonds. The strong intermolecular interaction resulted in the phase transformation from the liquid-state ionic liquids to solid-state crystals. The

[a]*NanoPowder and Thin Film Technology Center, ITRI South, Rm. 603, Bldg. R3, No. 31, Gongye 2nd Rd., Annan District, Tainan, Taiwan. E-mail: jasonyang0606@yahoo.com.tw; Fax: + 886 6 3847289; Tel: + 886 6 3847439*
[b]*Institute of Cosmetic Science, Chia Nan University of Pharmacy & Science, 60, Erh-Jen RD., Sec.1, Jen-Te, Tainan, Taiwan*

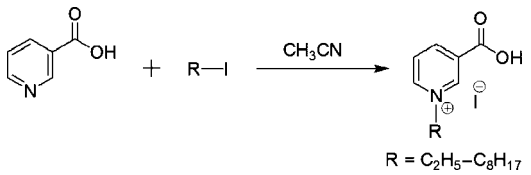

Scheme 1 Synthesis of 1-alkyl-3-carboxypyridinium iodides [ACP][I].

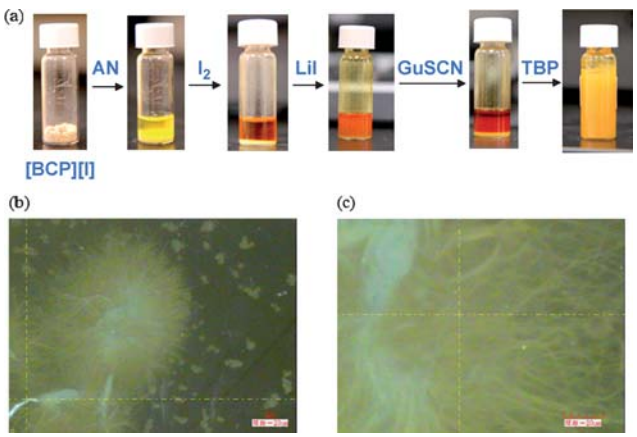

Fig. 1 (a) Photographs of the gel formed by electrolyte B. (b,c) Optical micrographs of microtubular structures formed in the platinized two-electrode cell.

molecular structures of the compounds were fully confirmed by ^{1}H NMR, ^{13}C NMR and elemental analysis.

The molten salt 1-butyl-3-carboxypyridinium iodide [BCP][I] was used. TBP, I_2 and LiI were dissolved in acetonitrile (AN) and valeronitrile (VN) (85 : 15, v/v) as a redox couple. After vigorous shaking of the electrolyte, a gel-state was formed without need for polymers or stiffeners (as shown in Fig. 1(a)). [BCP][I] is a small molecule that plays a role as a plasticizer and solidifies organic liquids by physically bonding with other constituents through H-bonding, van der Waals forces, and π–π bond stacking.[12] The intermolecular interactions between the constituents allows such molecules to self-assemble in solution, which can then trap solvent molecules and hence induce gelation. The microstructure of the gels was studied in platinized two-electrode cells by optical micrographs, which reveal the formation of a radiating fibrous network (Fig. 1(b,c)), consisting of numerous long fibers with diameters of 0.5–2 μm. The formation of numerous mircofibers is of great benefit to the diffusion coefficient of I_3^-, as is discussed in more detail below. However, we were unable to study the microstructure by scanning electron microscopy (SEM), because of the fast evaporation of the solvent that occurred from the gel in unsealed conditions.

We report for the first time the observation of self-assembled microfibrous structures from [ACP][I]–TBP–LiI–AN mixtures. We found the diffusion constant was strongly influenced by the generation of these microfibrous domains. The self-assembled microfibrous structure is probably caused by the pyridinium cations, TBP and LiI through H-bonding, van der Waals forces, π–π bond stacking and lithium coordination, and the probable mechanism is suggested in Fig. 2. The proposed self-assembled microfibrous unit contains one Li^+ cation, one pyridinium cation

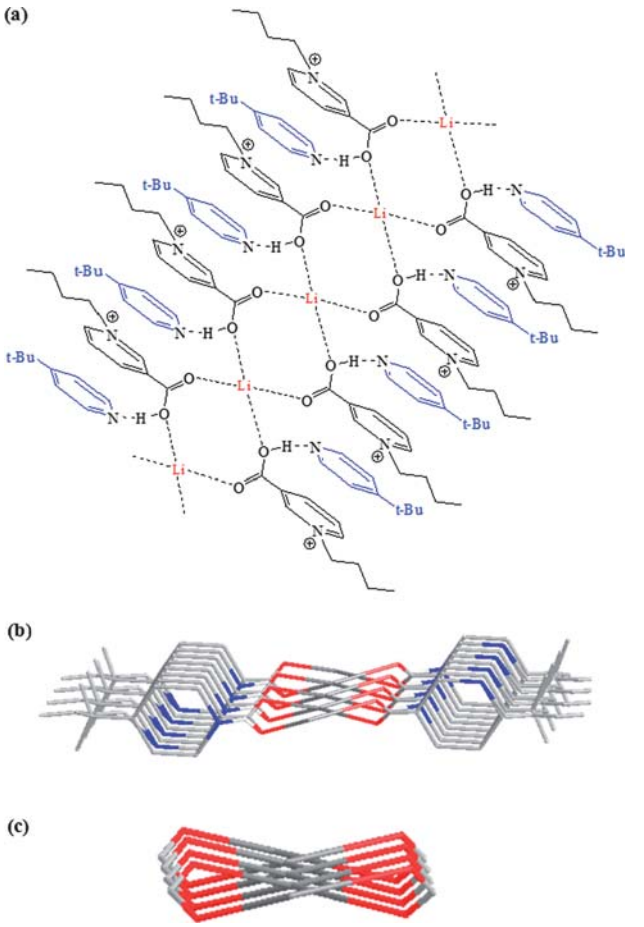

Fig. 2 Proposed structures of the microfibrous structures: (a) Chem-Draw representation of the microfibrous fragment. Chem 3D representations of the microfibrous fragment: (b) a side view, and (c) the inorganic chain. The red and blue labels are O and N atoms, respectively, and all of the hydrogen atoms, except those between ACPs and TBPs, are omitted for clarity.

(ACP) and one 4-*tert*-butylpyridine molecules (TBP). Each Li^+ cation is coordinated by O atoms of four different ACPs, leading to a distorted tetrahedral geometry, and each ACP bridges two different Li^+ cations with a hydrogen bond between TBP through the protonated O atom. The complicated structures formed by alkali metal complexes have been discussed extensively in the literature.[13] We presume that the proposed self-assembled microfibrous structure displays a similar polymeric configuration, consisting of infinite chains with alternating $[(ACP)(TBP)Li]^{2+}$ units in the presence of supramolecular interactions of hydrogen bonding and π–π stacking.

Recently, a solid crystalline compound $(MBI)_6(MBI\text{-}H^+)_2(I^-)(I_3^-)$ was isolated from various DSSC electrolytes containing MBI (*N*-methylbenzimidazole) as an additive.[14] Alternating iodide and linear triiodide anions form infinite chains along the crystallographic *a*-axis. We speculate that the self-assembled microfibrous structures play a similar role to the solid crystalline compound. The infinite chains of I^- and I_3^- along the microfibrous structures contribute to the diffusion constant of I_3^-, by producing something like a Grothuss-type, non-diffusional hopping mechanism. In combination with

I_3^- transport to the counter electrode by diffusion in AN, electrolyte B creates a surprisingly high diffusion constant.

Diffusion of iodide/triiodide in molten salt

Gel electrolytes consisting of ionic liquids, such as [PMI][I], and different gelators have previously been reported.[15–17] These gel electrolytes were injected into DSSCs, and exhibited poor performance compared to non-gelled ionic liquid electrolytes. The decrease in performance is associated with a decrease in diffusion properties of the redox species. The diffusion coefficient of I_3^- in gel electrolytes is about 10–20% lower than that in the corresponding ionic liquid electrolyte before gelation.[7] In this work, a gel electrolyte based on [BCP][I] has been used as a constituent of electrolytes for DSSC. We keep the volatile solvent (AN) in this electrolyte to ensure higher ionic conductivity and diffusion coefficients, and utilize [BCP][I] as the I^- source and gelator. To investigate the change in charge transfer and ionic transport processes in DSSCs, we carried out limiting current measurements and electrochemical impedance spectroscopy measurements. Limiting current density can be determined from cyclic voltammetry (CV) measurements of a two-electrode thin-layer cell. By using a slow scan rate (8 mV s^{-1}), very small hysteresis was observed under steady-state conditions.[18] The diffusion-limited current density (J_{lim}) is proportional to $D_{I_3^-}$, and is defined as

$$J_{lim} = \frac{2nFD_{I_3^-}C}{l} \quad (1)$$

where F is the Faraday constant, C is the initial concentration of iodine, l is the distance between the two electrodes and n is the electron transfer number.

Due to the large excess of I^- in the electrolyte, only the diffusion of I_3^- limits the current. By substitution of the J_{lim} obtained from CV measurements into eqn (1), the results for diffusion constants were obtained, and these are summarized in Table 1. As shown in Fig. 3, electrolyte B exhibited a similar steady-state current–voltage curve to electrolyte A. However, electrolyte C had the lowest J_{lim}, due to the nature of the electrolyte (based on methoxypropionitrile, MPN) compared to the AN-based electrolyte. For electrolytes A and C, the diffusion constant of I_3^- was 17.6×10^{-6} cm^2 s^{-1} and 5.6×10^{-6} cm^2 s^{-1}, respectively. These results agree with those for AN-based and MPN-based electrolytes in the literature.[19,20] Interestingly, electrolyte B had the highest diffusion constant of 28.5×10^{-6} cm^2 s^{-1}, and to the best of our knowledge, this is a new record for electrolytes in gel electrolytes. We speculate that the network of solidified electrolyte B will not affect the diffusion rate of I_3^- in acetonitrile to the counter electrode, and the formation of mircofibers, as noted above, was beneficial for I_3^- ionic transport by a Grothuss-type mechanism.

Table 1 Diffusion constant ($D_{I_3^-}$) and conductivity (σ) of different electrolytes

	$c_{I_3^-}$ (mol L^{-1})	$D_{I_3^-}$ (cm^2 s^{-1})	R_b (Ω cm^2)	σ (mS cm^{-1})
Electrolyte A	0.05	17.6×10^{-6}	0.95	6.34
Electrolyte B	0.03	28.5×10^{-6}	1.40	4.30
Electrolyte C	0.05	5.6×10^{-6}	6.59	0.91

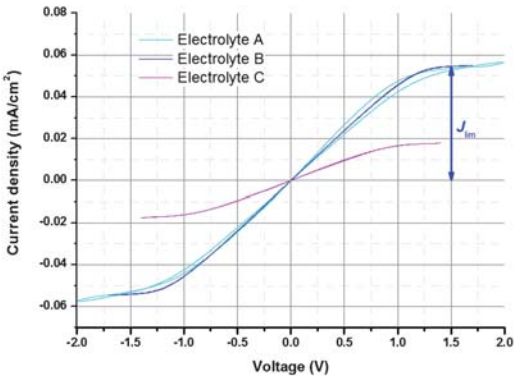

Fig. 3 Steady-state current–voltage curves of the electrochemical cells.

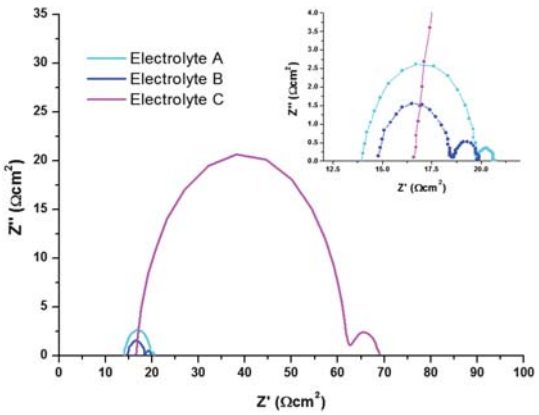

Fig. 4 Nyquist diagrams of the impedance spectra for different electrolytes sandwiched between planar Pt electrodes. The impedance element at high frequency is the Pt–electrolyte interface (charge-transfer resistance and double-layer capacitance), and at low frequency the Nernst diffusion impedance. The inset shows an enlarged view of electrolytes B and C.

Fig. 4 is the Nyquist spectrum of the platinized two-electrode cell with the iodide-based electrolytes. The spectrum consists of a semicircle in the high-frequency region, a slope of about 45° related to the Warburg impedance frequency region, and a semicircle in the low-frequency region. The response at high frequency can be attributed to the counter electrode–electrolyte interface, while the response at low frequency can be associated with the diffusion processes in the electrolyte. From the parameters obtained by fitting the experimental data, the conductivity (σ) can be estimated by using Ohm's law (eqn (2))[21]

$$\sigma = \frac{1}{R_b} \times \frac{t}{A} \quad (2)$$

where R_b is the resistance of the electrolyte, t is the thickness of the electrolyte film, and A is the area of the electrode.

The data for the Nyquist spectrum are summarized in Table 1. Fig. 4 shows that the overall impedance of the system decreases after changing the MPN-based electrolyte to an AN-based one. These data are in agreement with the decrease in viscosity of pure MPN (1.20 mPa s) and AN (0.34 mPa s), respectively.[22]

Table 2 Photovoltaic performance of DSSCs based on different electrolytes

Device (Electrolyte)	Thickness (μm)	V_{oc} (V)	J_{sc} (mA cm^{-2})	FF	η (%)
A (Solaronix AN-50)	8.0	0.80	6.8	0.74	4.0
B (Electrolyte B)	8.0	0.59	9.4	0.67	3.7
C (Electrolyte A)	12.0 + 4.0	0.75	14.8	0.62	6.9
D (Electrolyte B)	12.0 + 4.0	0.61	14.3	0.62	5.3
E (Electrolyte C)	12.0 + 4.0	0.58	15.4	0.48	4.3

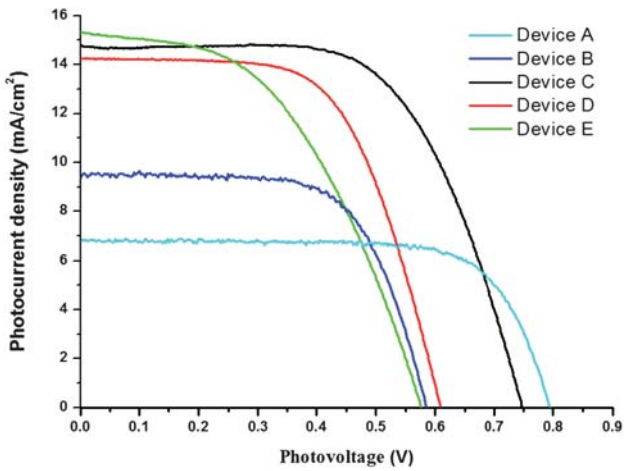

Fig. 5 Photocurrent density–voltage characteristics of DSSCs with different electrolytes under AM 1.5 illumination. The active area of the devices is 0.25 cm^2.

Electrolytes should have low viscosity to permit the rapid diffusion of charge carriers, and it is reasonable that liquid electrolyte A exhibited excellent ionic conductivity. Surprisingly, the conductivity value of gel electrolyte B was estimated as 4.30 mS cm^{-1}, which is very close to the value for a liquid electrolyte A, 6.34 mS cm^{-1}. As discussed before, this effect can be attributed to the viscosity of AN and the gel type network, which permits ionic species diffusion between the pores.

Photovoltaic properties

Under illumination of 100 mW cm^{-2}, the photovoltaic performances of DSSCs based on electrolytes A, B and C are shown in Table 2, while their photocurrent–voltage characteristics are presented in Fig. 5. Fig. 5 shows the photocurrent density *vs.* voltage response of two cells (devices A and B) made with 8 μm layers of TiO_2. In this case, device B shows a higher photocurrent density (9.4 mA cm^{-2}) than device A (6.8 mA cm^{-2}). The electrolyte used in device B was one which gives a lower voltage but promotes high quantum efficiency of electron injection for N719. Although electrolyte B achieved a lower voltage by moving the quasi-Fermi level of the TiO_2 layer (which resulted from the change in the flat-band potential (V_{fb}) of the TiO_2–electrolyte interface)[23,24] close to the iodide/triiodide couple and away from the excited state potential of N719, it exhibits a higher photocurrent density. Consequently, the result of the performance of device B (based on gel-electrolyte B) was comparable to that of device A (based on liquid electrolyte Solaronix AN-50) in the thinner devices.

For device C (which uses liquid electrolyte A), the photovoltaic performance parameters were in agreement with previous reports based on the liquid-type electrolyte. For device D (which uses 0.6 M [BCP][I] as the electrolyte), the efficiency η was 5.3%. This is the first time that such a high efficiency was obtained for a DSSC with this kind of gel-electrolyte under full sunlight. The use of the molten salt crystal [BCP][I] with iodine as an electrolyte for DSSC leads to a high short-circuit photocurrent density and a high light-to-electricity conversion efficiency. This is probably caused by a self-assembled microfibrous structure of the pyridinium cations, resulting in a high conductivity of the electrolyte.[25,26] In addition, compared to device D (which uses gel electrolyte B), device E (which uses gel electrolyte C) showed lower total conversion efficiencies, because of the enhanced back-transfer of injected electrons from the conduction band of TiO_2 film to the iodide/triiodide couple and the higher viscosity of MPN. This undesirable back-transfer and higher viscosity are also responsible for the lower V_{oc} value and FF, respectively.

One can see from Fig. 5 and Table 2 that the V_{oc} of devices B, D and E was only around 0.6 V by using [BCP][I] as the iodide source, but that the J_{sc} of these devices showed excellent performance compared to devices A and C, which were based on liquid electrolytes. This result suggests that the quasi-Fermi level of the TiO_2 layer moves downward relative to iodide/triiodide, which leads to a decrease in V_{oc}; but the diffusion of gel electrolyte is faster than that of the liquid electrolyte, which results in the enhancement of J_{sc}. This result is also in agreement with the observation of higher $D_{I_3^-}$ by using electrolyte B in Table 1. If the V_{oc} is optimized through varying the redox electrolyte composition, to the level of N719, *e.g.* >0.7 V, *ca.* 7% power-conversion efficiency can be anticipated for this device. Further efforts in this direction are still in progress in our laboratory.

Conclusions

The present results show that [ACP][I] can be used as an iodide source and a stiffener for gel electrolytes without any other plasticizers or nanoparticles. Compared with the commercial electrolyte Solaronix AN-50, this unique gel electrolyte enhances the short-circuit photocurrent density and light-to electricity conversion efficiency. These multifunctional molten salts are not only promising for gel electrolytes in DSSC, but also have potential for further innovations in electrolytes.

Experimental section

Materials and reagents

Transparent conducting oxide (TCO, F-doped SnO_2, 10 Ω per square, Solaronix SA) coated glass was used as the substrate for the TiO_2 thin-film electrode after detergent washing. Reagent grade LiI, I_2, 4-*tert*-butylpyridine (TBP), acetonitrile (AN) and methoxypropionitrile (MPN) were purchased from Aldrich and used without further purification. *cis*-Diisothiocyanato-bis(2,2′-bipyridyl-4,4′-dicarboxylato)ruthenium(II) bis(tetrabutylammonium) (N719), titania paste (Ti-Nanoxide T series) and iodide electrolyte (Iodolyte AN-50) were purchased from Solaronix SA. Nicotinic acid and alkyl iodides were purchased from TCI and Aldrich, respectively. [ACP][I] was prepared by a modified method presented in the literature,[11] and its purity was confirmed by analysis of the ^{1}H NMR and ^{13}C NMR spectra. The molecular structures of pyridinium iodides used in this work are shown in Scheme 1.

General procedure for the synthesis of [ACP][I]

Pyridine-3-carboxylic acid (nicotinic acid (1 equiv.)) was added to an ACE pressure tube together with alkyl iodide (2 equiv.) and acetonitrile (100 ml). After the cap was screwed on, the mixture was heated at 110 °C for 7 d. While the solution was cooling, ethyl acetate (EtOAc) was added to the mixture. The solid thus obtained was then filtered and washed with EtOAc, and dried under a vacuum.

Measurement of electrochemical characteristics

In this work the diffusion coefficients of the electrolytes were determined by limiting current measurements, with the triiodide being the current-limiting species.[18,27] Conductivity measurements were measured by electrochemical impedance spectroscopy (EIS) at frequencies ranging from 0.05 Hz to ~1 MHz. Electrochemical cyclic and linear sweep voltammetry and impedance spectra of electrolytes were measured using an Autolab Frequency Analyzer set-up, consisting of an Autolab PGSTAT 12 (Eco Chemie B.V., Utrecht, The Netherlands) producing a small amplitude harmonic voltage, and a Frequency Response Analyzer module. The experimental setup consisted of two platinized conducting glass electrodes separated by a 60 μm Surlyn sheet. The surface area of this cell was 1 cm^2, and the procedure was performed in an argon atmosphere in order to minimize any undesirable influences from the presence of residual atmospheric oxygen and water.

Fabrication of photovoltaic devices

8 μm nanocrystalline TiO_2 photoelectrodes were prepared from titania paste (Ti-Nanoxide T series, Solaronix SA). The paste was applied to the transparent conducting oxide by 'doctor-blading' techniques and annealed at 450 °C for 30 min in air. The thickness of the TiO_2 films was measured with an Alpha-Step 300 profiler. Once the TiO_2 electrodes had been cooled to around 100 °C, they were dipped in a 0.3 mM solution of N719 in *tert*-butanol–AN (1 : 1, v/v). The TiO_2 electrodes were immersed in the dye solutions and then kept at 25 °C for more than 12 h to allow the dye to adsorb on the TiO_2 surface, and rinsed with the same solvents. The dye-loaded TiO_2 film (as the working electrode) and Pt-coated TCO (as the counter electrode) were separated by a hot-melt Surlyn sheet (60 μm) and sealed together by pressing them under heat. The gel electrolytes were heated to 80 °C for a clear solution and introduced into the gap between the working and the counter electrodes from the two holes predrilled on the back of the counter electrode. Finally, the two holes were sealed with a Surlyn film covering a thin glass slide under heat. Three different electrolytes, A: 0.6 M [PMI][I] + 0.1 M LiI + 0.03 M I_2 + 0.5 M TBP in a mixture of acetonitrile and valeronitrile (85 : 15, v/v); B: 0.6 M [BCP][I] + 0.1 M LiI + 0.03 M I_2 + 0.5 M TBP in a mixture of acetonitrile and valeronitrile (85 : 15, v/v); C: 0.6 M [BCP][I] + 0.1 M LiI + 0.05 M I_2 + 0.5 M TBP in methoxypropionitrile, were used in this work.

Photovoltaic measurements

The current–voltage (*I–V*) characteristics in the dark and under illumination were measured with a Keithley 2400 sourcemeter. The photocurrent was measured in a nitrogen-filled glove box under a solar simulator (Oriel 96000 150W) with AM 1.5G-filtered illumination (100 mW cm^{-2}). The spectra-mismatch factor of the simulated solar irradiation was corrected using a Schott visible-color glass-filtered (KG5 color filter) Si diode (Hamamatsu S1133).[28] The active area of the device was 0.25 cm^2.

References

1 B. O'Regan and M. Gratzel, *Nature*, 1991, **353**, 737.
2 M. Gratzel, *J. Photochem. Photobiol., A*, 2004, **164**, 3.
3 A. F. Nogueira, J. R. Durrant and M. A. De Paoli, *Adv. Mater.*, 2001, **13**, 826.
4 T. Stergiopoulos, I. M. Arabatzis, G. Katsaros and P. Falaras, *Nano Lett.*, 2002, **2**, 1259.
5 A. B. F. Martinson, T. W. Hamann, M. J. Pellin and J. T. Hupp, *Chem. Eur. J.*, 2008, **14**, 4458.
6 J. N. De Freitas, A. F. Nogueira and M. A. De Paoli, *J. Mater. Chem.*, 2009, **19**, 5279.
7 M. Gorlov and L. Kloo, *Dalton Trans.*, 2008, 2655.
8 S. M. Zakeeruddin and M. Gratzel, *Adv. Funct. Mater.*, 2009, **19**, 2187.
9 Y. Bai, Y. Cao, J. Zhang, M. Wang, R. Li, P. Wang, S. M. Zakeeruddin and M. Grätzel, *Nat. Mater.*, 2008, **7**, 626.
10 Z. S. Wang, N. Koumura, Y. Cui, M. Miyashita, S. Mori and K. Hara, *Chem. Mater.*, 2009, **21**, 2810.
11 Z. M. Wang, C. N. Wang, W. L. Bao and T. K. Ying, *J. Chem. Res. (S)*, 2005, **2005**, 388.
12 N. M. Sangeetha and U. Maitra, *Chem. Soc. Rev.*, 2005, **34**, 821.
13 W. Clegg and L. Russo, *Cryst. Growth Des.*, 2009, **9**, 1158.
14 A. Fischer, H. Pettersson, A. Hagfeldt, G. Boschloo, L. Kloo and M. Gorlov, *Sol. Energy Mater. Sol. Cells*, 2007, **91**, 1062.
15 P. Wang, S. M. Zakeeruddin, J. E. Moser, M. K. Nazeeruddin, T. Sekiguchi and M. Gratzel, *Nat. Mater.*, 2003, **2**, 402.
16 P. Wang, S. M. Zakeeruddin, I. Exnar and M. Gratzel, *Chem. Commun.*, 2002, 2972.
17 P. Wang, S. M. Zakeeruddin, P. Comte, I. Exnar and M. Gratzel, *J. Am. Chem. Soc.*, 2003, **125**, 1166.
18 A. Hauch and A. Georg, *Electrochim. Acta*, 2001, **46**, 3457.
19 G. Oskam, B. V. Bergeron, G. J. Meyer and P. C. Searson, *J. Phys. Chem. B*, 2001, **105**, 6867.
20 R. Pereiro, A. J. Arvía and A. J. Calandra, *Electrochim. Acta*, 1972, **17**, 1723.
21 J. G. Webster, *Electrical Impedance Tomography*, Adam Hilger: Bristol/New York, 1990.

22 Ch. Wohlfarth, *Landolt-Bornstein – Group IV Physical Chemistry*, Springer, 2009.
23 M. S. Kang, J. H. Kim, J. Won and Y. S. Kang, *J. Phys. Chem. C*, 2007, **111**, 5222.
24 T. S. Kang, K. H. Chun, J. S. Hong, S. H. Moon and K. J. Kim, *J. Electrochem. Soc.*, 2000, **147**, 3049.
25 N. Yamanaka, R. Kawano, W. Kubo, T. Kitamura, Y. Wada, M. Watanabe and S. Yanagida, *Chem. Commun.*, 2005, 740.
26 N. Yamanaka, R. Kawano, W. Kubo, N. Masaki, T. Kitamura, Y. Wada, M. Watanabe and S. Yanagida, *J. Phys. Chem. B*, 2007, **111**, 4763.
27 N. Papageorgiou, Y. Athanassov, M. Armand, P. Bonhote, H. Pettersson, A. Azam and M. Gratzel, *J. Electrochem. Soc.*, 1996, **143**, 3099.
28 V. Shrotriya, G. Li, Y. Yao, T. Moriarty, K. Emery and Y. Yang, *Adv. Funct. Mater.*, 2006, **16**, 2016.